

Communication

Development and Characterization of Biomimetic Carbonated Calcium-Deficient Hydroxyapatite Deposited on Carbon Fiber Scaffold

Quentin Picard, Florian Olivier, Sandrine Delpeux, Jérôme Chancolon, Fabienne Warmont and Sylvie Bonnamy *

Centre National de la Recherche Scientifique (CNRS), University Orléans, ICMN UMR 7374, F-45071 Orléans, France; quentin.picard.pro@gmail.com (Q.P.); florian.olivier@cnrs-orleans.fr (F.O.); delpeux@cnrs-orleans.fr (S.D.); jerome.chancolon@cnrs-orleans.fr (J.C.); fabienne.warmont@cnrs-orleans.fr (F.W.)

* Correspondence: sylvie.bonnamy@cnrs-orleans.fr; Tel.: +33-023-825-5366

Received: 2 March 2018; Accepted: 12 April 2018; Published: 23 April 2018



Abstract: Calcium phosphate and derivatives have been known for decades as bone compatible biomaterials. In this work, the chemical composition, microtexture, and structure of calcium phosphate deposits on carbon cloths were investigated. Three main types of deposits, obtained through variation of current density in using the sono-electrodeposition technique, were elaborated. At low current densities, the deposit consists in a biomimetic, plate-like, carbonated calcium-deficient hydroxyapatite (CDA), likely resulting from the in situ hydrolysis of plate-like octacalcium phosphate (OCP), while at higher current densities the synthesis leads to a needle-like carbonated CDA. At intermediate current densities, a mixture of plate-like and needle-like carbonated CDA is deposited. This established that sono-electrodeposition is a versatile process that allows the coating of the carbon scaffold with biomimetic calcium phosphate while tuning the morphology and chemical composition of the deposited particles, thereby bringing new insights in the development of new biomaterials for bone repair.

Keywords: carbon scaffold; electrodeposition; calcium phosphates; carbonated calcium-deficient hydroxyapatite; carbon biomaterial

1. Introduction

Due to their mechanical properties, i.e., flexural and fatigue strength, and high strength to weight ratio, carbon fibers have previously been considered for hard and soft tissue engineering. However, their poor biological activity limits their extensive use in medical applications and therefore needs to be enhanced [1–3]. Conversely, owing to high biocompatibility, bioactivity, and osteoconductivity, calcium orthophosphate (CaP) ceramics, such as hydroxyapatite (HAP), have received much attention in the field of tissue engineering and have been clinically employed either as coating or as scaffold in orthopaedics and dentistry [3–5]. In this context, CaP-coated carbon fibers or cloth, combining the high biocompatibility of CaP with the properties of carbon fiber, appear as promising biomaterials for bone repair and regeneration [2,3,6].

In the past decades, several methods including plasma spray, radio-frequency sputtering, pulsed laser-deposition, sol-gel routes, electrophoretic methods, and electrochemical deposition have been reported for CaP deposition onto implant surfaces [5,7–9]. Among these, the electrochemical technique is particularly attractive for efficiently coating highly irregular materials at ambient temperatures and has been already applied for metal substrates or porous carbon composites [1–3,10–13]. Additionally, the thickness of the coating and its chemical composition can be well controlled by setting adequate

parameters [1,2,6,12–14]. The purpose of this present study is to demonstrate the effect of current density on thickness, morphology, microtexture, and chemical composition of the CaP phases deposited on carbon cloths in order to modulate these features according to desired application.

2. Materials and Methods

The substrate of the biomaterial is made of an activated carbon cloth (ACC). It is referred to as KIP1200 and was provided by Dacarb[®] (Asnières-sur-Seine, France).

CaP coating on the ACC is performed using a sono-electrochemical deposition method [1,15]. The electrolyte consisted of a calcium nitrate tetrahydrate $\text{Ca}(\text{NO}_3)_2 \cdot 4\text{H}_2\text{O}$, and ammonium dihydrogenophosphate $\text{NH}_4\text{H}_2\text{PO}_4$ mixture maintaining a Ca/P ratio of 1.67 with $[\text{Ca}^{2+}] = 5.10^{-3}$ mol/L. $\text{Hg}/\text{Hg}_2\text{SO}_4$ was used as reference electrode, and a (cd) ranging from 25 to 500 mA/g for 6 h. Sonication was applied during polarization in order to obtain a uniform and homogenous coating on the carbon fibers [16].

XRD was performed on an INEL diffractometer (CSP120) equipped with a curve detector (angular instrumental resolution of 0.05°) in transmission mode at copper wavelength (0, 154, 056 nm) with Si (111) monochromator. For the measurements, the samples were introduced in 0.6 mm diameter capillary glass tube. Scanning electron microscopy (SEM-Hitachi S4500, Tokyo, Japan), transmission electron microscopy (TEM-Philips CM20 working at 200 kV) associated with EDX analysis (EDAX detector, Eindhoven, The Netherlands), elemental analysis (Flash 2000, Thermo Scientific France, Courtabœuf, France), and N_2 and CO_2 adsorption, respectively, at 77 and 273 K (Autosorb-1, Quantachrome France, Bailleau le Pin, France), were performed to characterize the carbon cloth substrate along with the chemical composition, morphology, microtexture, and structure of the CaP deposits.

3. Results

3.1. Characteristics of Carbon Fiber Scaffold

The carbon fiber scaffold is made of 10 μm diameters woven fibers as seen on SEM image (Figure 1a).

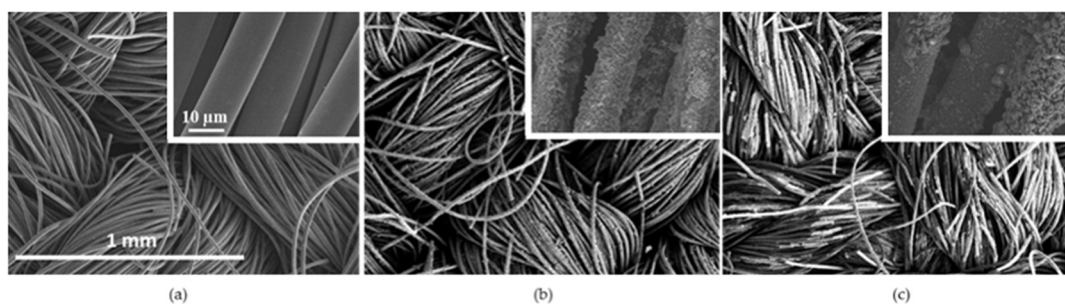


Figure 1. SEM micrographs of (a) pristine activated carbon fiber cloth; (b) CaP coated carbon cloth with homogeneous (as an example at 75 mA/g); and (c) heterogeneous (as an example at 25 mA/g) coverage of the fibers. Insets are given higher magnifications of the carbon fibers.

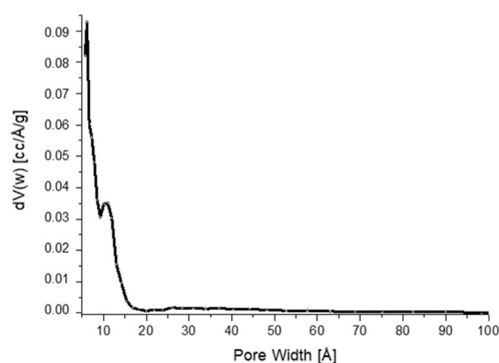
Elemental analysis of the carbon cloth was performed to determine the proportion of elemental atoms (mass %). It contains 92.4% of carbon, 1.6% of oxygen, 0.6% of hydrogen, and about 5% of ashes. The material is rather hydrophobic, since it presents a low amount of oxygen, and consequently of oxygenated surface groups, and its zero charge pH is basic, equal to 9.4.

The activated carbon fiber cloth possesses a highly developed surface area (Table 1). Its porous network consists of micropores (7–20 Å) and ultramicropores (<7 Å). The material presents a narrow pore size distribution centered at 10–12 Å (Figure 2).

Table 1. Microtextural and nanotextural KIP1200 characteristics.

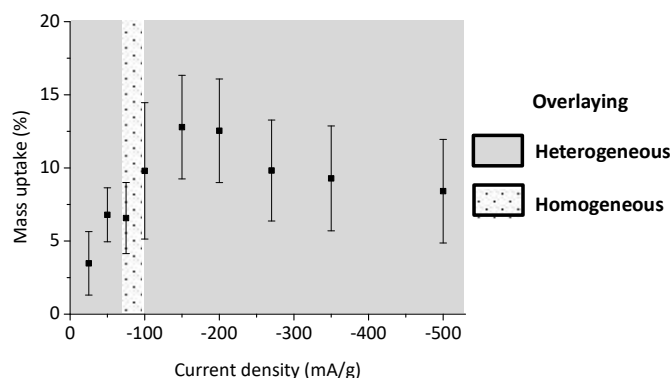
S_{BET} (m^2/g)	V_{total} (cm^3/g)	V_{micro}^1 (cm^3/g)	$V_{\text{ultramicro}}^2$ (cm^3/g)	V_{meso}^1 (cm^3/g)
1693	0.68	0.51	0.52	0.09

¹ Measured by N_2 adsorption at 77 K, using the density functional theory (DFT) method. ² Measured by CO_2 adsorption at 273 K, using the Dubinin-Radushkevich (DR) theory.

**Figure 2.** Pore size distribution of KIP1200 activated carbon cloth (N_2 adsorption at 77 K).

3.2. Homogeneity of the CaP Deposits

The variation of the mass uptake as a function of the applied current density is reported in Figure 3. A 13% maximum mass uptake is reached at 150 mA/g. The deposit thickness was measured after fracture of the fibers under liquid nitrogen. The homogeneity vs heterogeneity of the coating was determined on transversal sections of carbon fibers observed at higher magnification in SEM (see insets in Figure 1).

**Figure 3.** Variation of the mass uptake as a function of applied current density. Error bars are calculated according to student test with five experimental points.

For current densities in order of 75 mA/g, the CaP deposit appears rather homogeneous (see inset in Figure 1b) with a thickness ranging from 250 to 600 nm. At other current densities, CaP coverage of the fibers is heterogeneous. At low current densities (25 and 50 mA/g) (see inset in Figure 1c), the deposit is irregular, and its thickness is smaller than 100 nm, whereas for higher current densities (100 and 270 mA/g), the deposit is highly heterogeneous and its thickness ranges from 600 nm to 2 μm .

The amount and homogeneity of the CaP deposits thus showed a strong dependency on the water electrolysis regime, governed by the current density applied at the negative electrode. The water electrolysis regime is -0.94 V at pH of 4.8. Water reduction occurring at the carbon cathode surface enhances hydroxyl anions production according to reaction (1):



The mass uptake and the homogeneity of the deposit then depend on the proportion of H_2 (g) and OH^- production. While below 150 mA/g the amount of deposit increases gradually with the OH^- production, the formation of H_2 bubbles in the carbon porosity for higher current densities reduces the surface contact between the carbon electrode and the electrolyte and avoids the CaP deposit formation. Consequently, a decrease of the deposit mass uptake is observed for current densities higher than 150 mA/g (Figure 3), associated with a heterogeneous and uncomplete CaP coverage on overlaying fibers, as seen on SEM image (Figure 1c and inset).

3.3. Microtexture of the CaP Deposits

TEM characterization shows that the microtexture of the deposit also depends on the applied current density. Below 50 mA/g, a plate-like microtexture is observed (Figure 4a), while for current densities above 100 mA/g, the deposits display a needle-like microtexture (Figure 4c). At 75 mA/g, both microtextures were observed simultaneously (Figure 4b). These results clearly indicate that depending on the current density, CaP deposits with two different types of microtextures could be obtained.

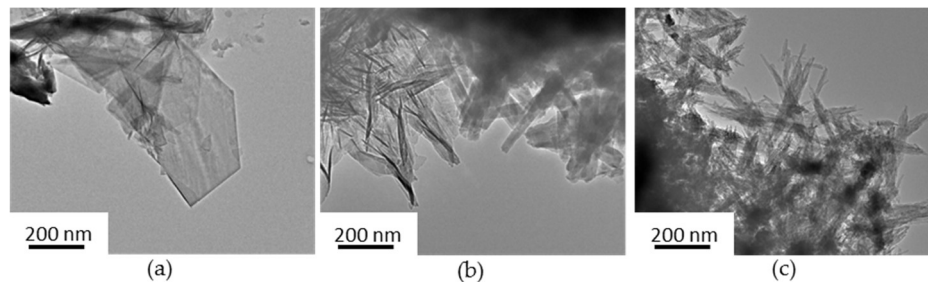


Figure 4. TEM micrographs of CaP deposits: (a) plate-like microtexture obtained at $cd \leq 50$ mA/g; (b) mixture between plate-like and needle-like microtextures obtained at 75 mA/g; and (c) only needle-like microtexture obtained at $cd \geq 100$ mA/g (magnification $\times 20,000$).

Because the current density governs the water electrolysis regime, it governs the microtexture of the CaP deposits. At high current densities (100 and 270 mA/g), the fast water electrolysis rate induces a strong pH increase, which favours PO_4^{3-} species and a direct precipitation of CaP deposits having a needle-like microtexture. At lower current densities (25 and 50 mA/g), the slow water electrolysis rate leads to a weak pH increase, which allows the simultaneous existence of HPO_4^{2-} and PO_4^{3-} ions. In this case, the deposit consists mainly in CaP deposits with a plate-like microtexture.

3.4. Chemical Composition of the CaP Deposits

In order to analyze the chemical composition of deposits, Ca/P atomic ratios were determined from EDX-TEM analysis at each current density (Figure 5).

Average Ca/P ratios are (1.40 ± 0.08) , (1.44 ± 0.04) , (1.68 ± 0.14) , and (1.62 ± 0.11) at, respectively, 25, 50, 75, and 100 mA/g. At 270 mA/g, two distinct Ca/P ratios are observed: (1.71 ± 0.08) and (2.3 ± 0.3) . From 25 to 270 mA/g, the Ca/P ratios increase. At 25 mA/g, Ca/P ratios are close to octacalcium phosphate (OCP) one (1.33) [17], which is coherent with the plate-like morphology observed at this current density. From 75 to 270 mA/g, Ca/P ratios increase from 1.44 to 1.71. It is worthwhile noticing that Ca/P ratio is 1.67 for stoichiometric hydroxyapatite (HAP) and ranges from 1.5 to 1.67 for calcium-deficient hydroxyapatite (CDA) [17], which is coherent with a needle-like morphology. Intermediate ratios observed at 50 mA/g can be explained by a mixture between OCP and HAP phases. The second Ca/P ratio of 2.3 obtained at 270 mA/g is explained by the mixture between HAP and calcite CaCO_3 observed by XRD (Figure 6).

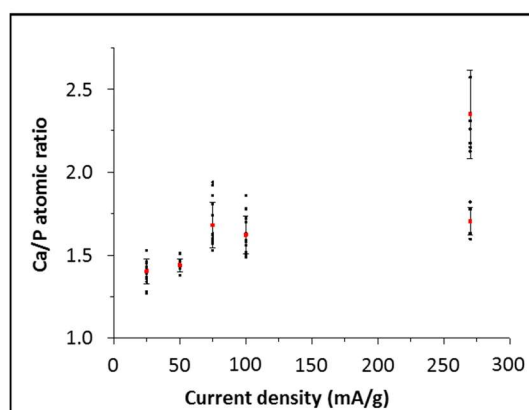


Figure 5. Ca/P atomic ratios obtained from EDX-TEM analysis as a function of the current density.

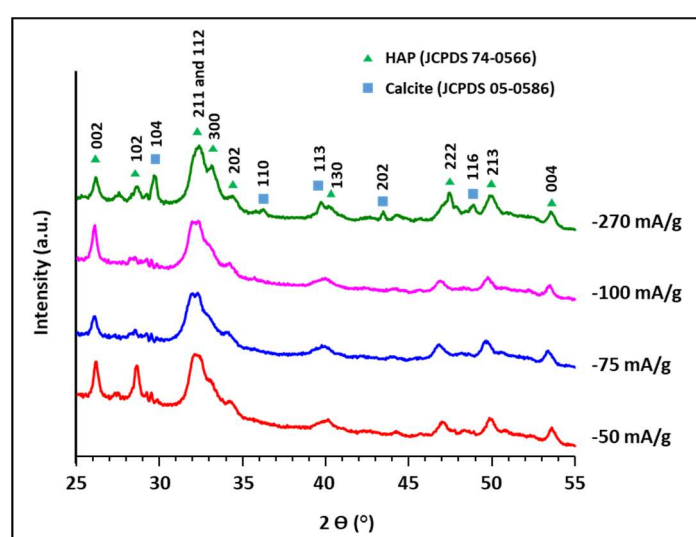


Figure 6. X-ray patterns of CaP deposits obtained at 50, 75, 100, and 270 mA/g ($K\alpha_{Cu} = 0.154056$ nm).

3.5. Identification of the CaP Phases

X-ray diffraction was performed to identify the crystallographic structure of the CaP deposits (Figure 6). XRD patterns of deposits obtained from 50 to 270 mA/g show broad main peaks located at $2\theta = 25.9^\circ, 32.9^\circ$, close to reflexions of stoichiometric hydroxyapatite (JCPDS 74-0566). They correspond to (002), (211), and (300) reflexions and are typical of a calcium-deficient hydroxyapatite (CDA) [18]. Broad peaks are due to a crystalline disorder induced by the partial substitution of phosphate and hydroxyls ions by carbonate ions [18] and by the nanometric size of crystallites. Only at 270 mA/g current density several other peaks are observed at $29.4^\circ, 36.0^\circ$ and 39.4° , which are characteristics of calcite allotropic form (JCPDS 05-0586).

To characterize the nature of the formed CaP phases present in the deposits, FTIR analyses were also performed (Figure 7a).

For current densities ranging from 50 to 270 mA/g, the FTIR spectra are clearly characteristic of carbonated calcium-deficient hydroxyapatite (CDA) [19].

The stretching band at 3540 cm^{-1} and the bending band at 633 cm^{-1} are associated with apatitic OH^- groups. The most intense and broad band centred at 1036 cm^{-1} with the shoulder at 1094 cm^{-1} and the double-band at 566 and 603 cm^{-1} with the shoulder at 580 cm^{-1} are characteristic of the ν_3 and ν_4 bending mode of apatitic PO_4^{3-} tetrahedra, respectively. The presence of carbonates is indicated by the ν_3 bands of the C–O bond in the $1410\text{--}1460\text{ cm}^{-1}$ region. The band at 871 cm^{-1} is

assigned either to ν_2 vibrations of C–O in CO_3^{2-} or to HPO_4^{2-} groups [2]. Finally, the broad bands in the ranges 1600–1800 and 2500–3700 cm^{-1} on all spectra are attributed to adsorbed water molecules in the carbonated CDA [19,20]. At a current density of 25 mA/g, the ν_3 PO_4^{3-} most intense peak centred at 1036 cm^{-1} shows a splitting with the appearance of bands at 916, 1025, and 1193 cm^{-1} characteristic of octacalcium phosphate (OCP) [19] (Figure 7b). The signature of carbonates is present in the 1410–1460 cm^{-1} region. Since carbonated OCP is unlikely to occur [21], this suggests that the deposit is a mixture of OCP and carbonated CDA. Carbonates ions are provided by atmospheric CO_2 solubilized in the electrolyte. Under sonication, a slight increase of the electrolyte temperature takes place (up to $\sim 44^\circ\text{C}$), which promotes the reaction of carbon dioxide and water molecules to form CO_3^{2-} , according to (2)–(4) [22]:

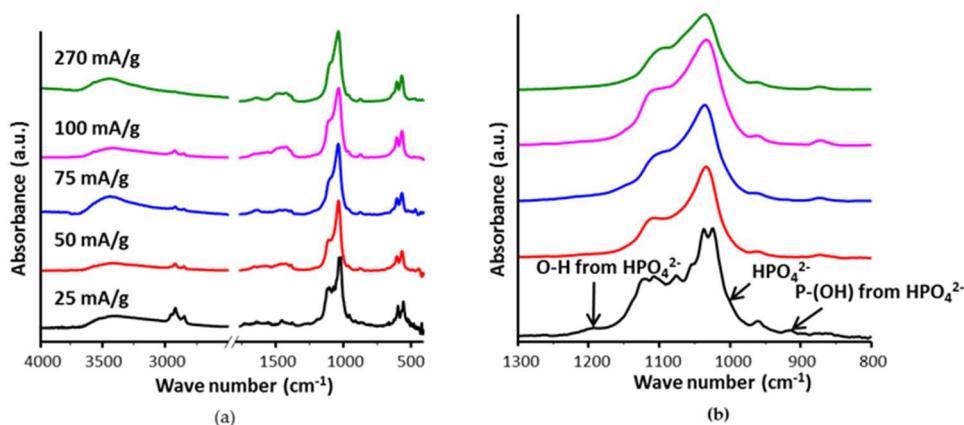
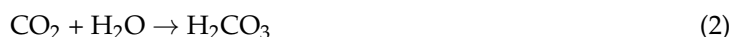


Figure 7. FTIR spectra of CaP deposits: (a) full spectra and (b) expansion of the ν_1 – $\nu_3\text{PO}_4^{3-}$ region.

4. Discussion

All the results demonstrate that, at high current densities (100 and 270 mA/g), the fast water electrolysis rate induces a strong pH increase that favours PO_4^{3-} species and gives rise to a direct precipitation of carbonated calcium-deficient hydroxyapatite (CDA) with needle-like morphology. In contrast, at lower current densities (25 and 50 mA/g), the slow water electrolysis rate only leads to a weak pH increase, which allows the simultaneous existence of HPO_4^{2-} and PO_4^{3-} ions. In this case, the deposit consists mainly in CDA (and disordered octacalcium phosphate (OCP) to a lower extent) with a plate-like morphology. This suggests that CDA formation onto the carbon fibers occurred in a different manner, likely through the precipitation of plate-like triclinic OCP, which is in situ converted into plate-like hexagonal CDA according to the reaction (5):



According to Brown et al. [23], the OCP hydrolysis into CDA is supported by a lattice reorganization through the losses of water, phosphate ions, or, eventually, calcium ions. As a consequence, structural defects and additional ions, such as carbonate groups, are incorporated in the hydroxyapatite structure.

The occurrence of such mechanism at low current densities allows for the explaining of the observation of plate-like carbonated CDA with a little amount of non-hydrolysed OCP at 25 mA/g. This OCP hydrolysis rate is expected to increase with the current density, and when it reaches 50 mA/g, the amount of non-hydrolysed OCP is too small to be evidenced by FTIR. It should be mentioned

that this OCP hydrolysis mechanism was postulated to be at the origin of plate-like carbonated CDA observed in bones [23,24]. At intermediate current density (75 mA/g), the coexistence of plate-like and needle-like morphologies suggests that the two mechanisms of CDA formation take place simultaneously. When electrolysis starts, the pH increase leads to plate-like OCP precipitation, which then is further hydrolysed into CDA, and later on, to needle-like carbonated CDA precipitation when the pH becomes sufficiently high.

5. Conclusions

Calcium phosphate coated-activated carbon cloths have been successfully devised using the sono-electrochemical deposition technique. This method allows one to increase the local pH of the electrolyte near the carbon electrode using water electrolysis, which drives the precipitation of calcium phosphate phases onto carbon fibers. Homogeneous coating with thicknesses ranging from 250 to 600 nm can be obtained using selected current charge densities. A thorough investigation of the coating mechanism and resulted CaP characteristics allow concluding on the current density-dependence of the deposit microtexture, structure, and chemical composition. At lower current density (25 mA/g), the deposit consists of disordered triclinic octacalcium phosphate (OCP) having a plate-like morphology, which is quickly in situ hydrolysed into disordered hexagonal calcium-deficient hydroxyapatite (CDA); the structure changes, but the plate-like microtexture is kept. As the current density increases (50 mA/g), the pH increase leads to losses of phosphate ions and to an increase of the OCP hydrolysis rate into carbonated CDA. At this stage, only particles of CDA having a plate-like microtexture (no more OCP particles) are observed. At high current densities (100 and 270 mA/g), the fast water electrolysis rate leads to a direct precipitation of carbonated CDA having a classical, needle-like microtexture.

It has been shown that using well defined experimental conditions, carbon fiber cloths can be coated with biomimetic carbonated CDA, which might be beneficial for use as a scaffold for bone regeneration. Biocompatibility and bioactivity tests are currently under progress to assess the biological properties of these novel and promising biomaterials [25,26].

Acknowledgments: This work was supported by the FP7-IRSES European program “ABREM” 2012–2015 and the Region Centre-Val de Loire project “MatBioReOs” 2013–2016.

Author Contributions: Quentin Picard performed the experiments; Quentin Picard and Florian Olivier have received a PhD grant from MESRI-France, Fabienne Warmont performed TEM images and Quentin Picard, Florian Olivier, Sandrine Delpoux, Jérôme Chancolon, and Sylvie Bonnamy wrote the paper.

Conflicts of Interest: The authors declare no conflict of interest.

References

1. Han, H.; Mikhailovsky, S.V.; Phillips, G.J.; Lloyd, A.W. Calcium phosphate sonoelectrodeposition on carbon fabrics and its effect on osteoblast cell viability in vitro, *New Carbon Mater.* **2007**, *22*, 121–125. [[CrossRef](#)]
2. Stoch, A.; Brożek, A.; Błażewicz, S.; Jastrzębski, W.; Stoch, J.; Adamczyk, A.; Rój, I. FTIR study of electrochemically deposited hydroxyapatite coatings on carbon materials. *J. Mol. Struct.* **2003**, *651–653*, 389–396. [[CrossRef](#)]
3. Kuo, M.C.; Yen, S.K. The process of electrochemical deposited hydroxyapatite coatings on biomedical titanium at room temperature. *Mater. Sci. Eng. C* **2002**, *20*, 153–160. [[CrossRef](#)]
4. Habraken, W.; Habibovic, P.; Epple, M.; Böhnerdoi, M. Calcium phosphates in biomedical applications: Materials for the future? *Mater. Today* **2016**, *19*, 69–87. [[CrossRef](#)]
5. Szcześ, A.; Hołysz, L.; Chibowski, E. Synthesis of hydroxyapatite for biomedical applications. *Adv. Colloid Interface Sci.* **2017**, *249*, 321–330. [[CrossRef](#)] [[PubMed](#)]
6. Han, H.M.; Phillips, G.J.; Mikhailovsky, S.V.; FitzGerald, S.; Lloyd, A.W. Sono-electrochemical deposition of calcium phosphate coatings on carbon materials—Effect of electrolyte concentration. *J. Mater. Sci. Mater. Med.* **2008**, *19*, 2845–2850. [[CrossRef](#)] [[PubMed](#)]

7. Yamashita, K.; Kitagaki, K.; Umegaki, T. Thermal instability and proton conductivity of ceramic hydroxyapatite at high temperatures. *J. Am. Ceram. Soc.* **1995**, *78*, 1191–1197. [[CrossRef](#)]
8. Yamashita, K.; Yonehara, E.; Ding, X.; Nagai, M.; Umegaki, T.; Matsuda, M. Electrophoretic coating of multilayered apatite composite on alumina ceramics. *J. Biomed. Mater. Res.* **1998**, *43*, 46–53. [[CrossRef](#)]
9. Candidato, R.T., Jr.; Sokolowski, P.; Pawlowski, L.; Lecomte-Nana, G.; Constantinescu, C.; Denoirjean, A. Development of hydroxyapatite coatings by solution precursor plasma spray process and their microstructural characterization. *Surf. Coat. Technol.* **2017**, *318*, 39–49. [[CrossRef](#)]
10. Ślósarczyk, A.; Klisch, M.; Błażewicz, M.; Piekarczyk, J.; Stobierski, L.; Rapacz-Kmita, A. Hot pressed hydroxyapatite–carbon fibre composites. *J. Eur. Ceram. Soc.* **2000**, *20*, 1397–1402. [[CrossRef](#)]
11. Metoki, N.; Mandler, D.; Eliaz, N. Effect of decorating titanium with different self-assembled monolayers on the electrodeposition of calcium phosphate. *Cryst. Growth Des.* **2016**, *16*, 2756–2764. [[CrossRef](#)]
12. Han, H.M.; Phillips, G.J.; Mikhalovsky, S.V.; FitzGerald, S.; Lloyd, A.W. Sono-electrochemical deposition of calcium phosphates on carbon materials: Effect of current density. *J. Mater. Sci. Mater. Med.* **2008**, *19*, 1787–1791. [[CrossRef](#)] [[PubMed](#)]
13. Musiani, M. Electrodeposition of composites: An expanding subject in electrochemical materials science. *Electrochim. Acta* **2000**, *45*, 3397–3402. [[CrossRef](#)]
14. Đoši, M.; Erakovi, S.; Jankovi, A.; Vukašinovi-Sekuli, M.; Mati, I.Z.; Stojanovi, J.; Rhee, K.Y.; Miškovi-Stankovi, V.; ParK, S.J. In vitro investigation of electrophoretically deposited bioactive hydroxyapatite/chitosan coatings reinforced by grapheme. *J. Ind. Eng. Chem.* **2017**, *47*, 336–347. [[CrossRef](#)]
15. Nardecchia, S.; Serrano, M.C.; Gutiérrez, M.C.; Portolés, M.T.; Ferrer, M.L.; del Monte, F. Osteoconductive performance of carbon nanotube scaffolds homogeneously mineralized by flow-through electrodeposition. *Adv. Funct. Mater.* **2012**, *22*, 4411–4420. [[CrossRef](#)]
16. Picard, Q. Biomatériaux hybrides: Tissu de fibres de carbone/phosphates de calcium: Synthèse, caractérisation et biocompatibilité. Ph.D. Thesis, Orléans University, Orléans, France, 30 November 2016.
17. Elliot, J.C. Structure and chemistry of the apatites and other calcium orthophosphates. *Stud. Inorg. Chem.* **1994**, *18*, 389–398.
18. Venkateswarlu, K.; Sandhyarani, M.; Nellaippan, T.A.; Rameshbabu, N. Estimation of crystallite size, lattice strain and dislocation density of nanocrystalline carbonate substituted hydroxyapatite by X-ray peak variance analysis. *Procedia Mater. Sci.* **2014**, *5*, 212–221. [[CrossRef](#)]
19. Karampas, I.A.; Kontoyannis, C.G. Characterization of calcium phosphates mixtures. *Vib. Spectrosc.* **2013**, *64*, 126–133. [[CrossRef](#)]
20. Raynaud, S.; Champion, E.; Bernache-Assollant, D.; Thomas, P. Calcium phosphate apatites with variable Ca/P atomic ratio I. Synthesis, characterization and thermal stability of powders. *Biomaterials* **2002**, *23*, 1065–1072. [[CrossRef](#)]
21. Gómez-Morales, J.; Iafisco, M.; Delgado-López, J.M.; Sarda, S.; Drouet, C. Progress on the preparation of nanocrystalline apatites and surface characterization: Overview of fundamental and applied aspects. *Prog. Cryst. Growth Charact. Mater.* **2013**, *59*, 1–46. [[CrossRef](#)]
22. Drevet, R. Élaboration de Nouveaux Revêtements Prothétiques Phosphocalciques par électrodéposition. Caractérisations Physico-chimique et Structurale. Ph.D. Thesis, Reims University, Reims, France, 10 June 2011.
23. Brown, W.E.; Smith, J.P.; Lehr, J.R.; Frazier, A.W. Octacalcium Phosphate and Hydroxyapatite: Crystallographic and Chemical Relations between Octacalcium Phosphate and Hydroxyapatite. *Nature* **1962**, *196*, 1050–1055. [[CrossRef](#)]
24. Brown, W.E.; Eidelman, N.; Tomazic, B. Octacalcium phosphate as a precursor in biomineral formation. *Adv. Dent. Res.* **1987**, *1*, 306–315. [[CrossRef](#)] [[PubMed](#)]
25. Han, H.M.; Phillips, G.J.; Mikhalovsky, S.V.; Lloyd, A.W. In vitro cytotoxicity assessment of carbon fabric coated with calcium phosphate. *New Carbon Mater.* **2008**, *23*, 139–143. [[CrossRef](#)]
26. Xie, W.; Song, F.; Wang, R.; Sun, S.; Li, M.; Fan, Z.; Liu, B.; Zhang, Q.; Wang, J. Mechanically robust 3D graphene-hydroxyapatite hybrid bioscaffolds with enhanced osteoconductive and biocompatible performance. *Crystals* **2018**, *8*, 105. [[CrossRef](#)]

